ADVANCED FUNCTIONAL MATERIALS
www.afm-journal.de

High-Fidelity Directed Self-Assembly Using Higher-χ Polystyrene-*Block*-Poly(Methyl Methacrylate) Derivatives for Dislocation-Free Sub-10 nm Features

*Shinsuke Maekawa, Lander Verstraete, Hyo Seon Suh, Takehiro Seshimo, Takahiro Dazai, Kazufumi Sato, Kan Hatakeyama-Sato, Yuta Nabae, and Teruaki Hayakawa**

Extreme ultraviolet (EUV) lithography currently enables the creation of ultrafine patterns. However, as miniaturization progresses, stochastic defects become a significant challenge. Directed self-assembly (DSA) of block copolymers (BCPs) has gained attention for pattern rectification to improve the quality of EUV patterns or for density multiplication to obtain sub-10 nm features. DSA is one of the most promising miniaturization processes because it does not cause stochastic defects. However, dislocation defects are an important issue in density multiplication using strongly segregating BCP. This study demonstrates the use of DSA on 300 mm silicon wafers with higher-Flory-Huggins interaction parameter (χ) polystyrene-*block*-poly(methyl methacrylate) derivatives for sub-10 nm features. These higher-χ polymers, synthesized from polystyrene-*block*-[poly(glycidyl methacrylate)-*random*-poly(methyl methacrylate)] (PS-*b*-PGM) and 2,2,2-trifluoroethanethiol (PS-*b*-PG_FM), show excellent reproducibility of perpendicular lamellae. Line patterns with a sub-10 nm half-pitch are successfully formed by DSA on 300 mm wafers. Line patterns without parallel-oriented structures or dislocations can be achieved by optimizing the chemical guides and annealing conditions. A polymer with a higher χN value exhibits improved roughness in the resulting line patterns.

1. Introduction

The demand for semiconductor chips has increased with the development of electronic devices and artificial intelligence. Extreme ultraviolet (EUV) lithography yields the smallest current pitch size.[1] The theoretical pattern pitch is expected to decrease to a sub-10 nm half pitch as EUV exposure equipment evolves.[2] Advancements in photoresists tailored for EUV lithography have significantly facilitated the miniaturization of circuit patterns.[3–10] However, a serious issue arises: as the pitch size decreases, the quality of the patterns may deteriorate owing to stochastic defects caused by photon shot noise, which is the relative uncertainty of the number of photons absorbed by the photoresists.[11–15] EUV exposure followed by directed self-assembly (DSA) of block copolymers (BCPs) has attracted attention as a method for producing more uniform patterns.[16–22] Another approach to obtain smaller uniform patterns is density multiplication by DSA.[16,23–25] Density multiplication does not require expensive EUV lithography or complex multipatterning approaches, as fine patterns can be obtained by ArF immersion lithography followed by DSA. BCPs form microphase-separated structures with periodic lengths ranging from a few to tens of nanometers, depending on key parameters such as the degree of polymerization (N), volume fraction (f), and Flory–Huggins interaction parameter (χ), of the polymers.[26–28] Perpendicular lamellae in BCP thin films on semiconductor substrates can serve as templates for line-and-space pattern transfers.[29–32] DSA methods

S. Maekawa, K. Hatakeyama-Sato, Y. Nabae, T. Hayakawa
Department of Materials Science and Engineering
School of Materials and Chemical Technology
Institute of Science Tokyo
2-12-1-S8-36 Ookayama, Meguro-ku, Tokyo 152-8552, Japan
E-mail: hayakawa.t.ac@m.titech.ac.jp

The ORCID identification number(s) for the author(s) of this article can be found under https://doi.org/10.1002/adfm.202421066

L. Verstraete, H. S. Suh
IMEC
Kapeldreef 75, Leuven 3001, Belgium

T. Seshimo, T. Dazai, K. Sato
Research & Development Department
Tokyo Ohka Kogyo Co., Ltd
1590 Tabata, Samukawa-machi, Koza-gun, Kanagawa 253-0114, Japan

DOI: 10.1002/adfm.202421066

include graphoepitaxy,[33–35] electric field,[36] roll casting,[37] and zone casting.[38,39] Chemoepitaxy, which uses chemical guides patterned on wafers, is a DSA method used to align perpendicular lamellae in thin films on wafers in the desired directions.[40,41] The patterns in the BCP thin films are defined by the self-assembly process; therefore, the photon-shot noise of the EUV is avoided.[20]

Polystyrene-*block*-poly(methyl methacrylate) (PS-*b*-PMMA) has been widely used in DSA studies[41–43] because perpendicular lamellae form in thin films owing to the similar air affinities of the blocks.[44] A chemoepitaxy process for PS-*b*-PMMA has been developed on an industrial scale.[23,45] However, the smallest pitch size transferred from PS-*b*-PMMA line patterns is 22 nm owing to the lower-χ value.[46] To achieve a sub-10 nm half pitch, BCPs with higher χ values have been reported. Although sub-10 nm half pitches have been succeeded by density multiplication using some high-χ BCPs,[47,48] reducing the number of structural defects is still one of the challenges. Optimization of the primary structure of the BCP and DSA process is a promising solution to obtain high-quality patterns. Achieving sub-10 nm half-pitch requires large density multiplication factors, resulting in an increase in dislocation density.[49] Density multiplication with high-χ BCPs is not easy to achieve patterns free of dislocation defects and may require long annealing times that are not practical for industry. Therefore, in order to obtain line patterns without dislocations in a short annealing time, the development of materials based on the understanding of the relationship between the repulsion of the blocks in the BCP, some parameters of the DSA process, and structural defects in the resulting patterns is extremely important. Doise et al. reported the correlation of the χN value of the high-χ BCP, each parameter of the DSA process, and dislocation densities, achieving 0–3 $\times$ 10^4 dislocations per cm^2.[50] However, the DSA process was modified from the conventional one developed using PS-*b*-PMMA, and a top-coat layer, which neutralizes the polymer/air interface, was required for the perpendicular orientation of lamellar structures.

We previously reported polystyrene-*block*-[poly(glycidyl methacrylate)-*random*-poly(methyl methacrylate)] (PS-*b*-(PGMA-*r*-PMMA) or PS-*b*-PGM) and its derivative functionalized with 2,2,2-trifluoroethenethiol (PS-*b*-PG_FM) as higher-χ PS-*b*-PMMA derivatives.[51] These polymers were used to precisely control the number of functional groups in the PG_FM block to realize strong segregation while balancing the air affinities of both blocks. The χ value of the polymer can be controlled by adjusting the ratio of functional group incorporation. A 15.1 nm pitch line pattern has been achieved via DSA without a topcoat for density multiplication. However, some structural defects were observed in the resulting patterns.

We performed DSA studies using PS-*b*-PG_FMs on 300 mm silicon wafers to obtain sub-10 nm half-pitch line patterns without defects, such as parallel-oriented structures to the wafers (parallel areas) and dislocations, by optimizing the chemical guides and annealing conditions. Prior to the DSA studies, we determined the perpendicular windows of the random copolymer composition as neutral layers and the thickness of the BCP thin films to investigate the reproducibility of the perpendicular lamellae in PS-*b*-PG_FM. Based on these perpendicular windows, DSA was performed on 300 mm silicon wafers by the established process based on PS-*b*-PMMA. We optimized the pitch size (L_s) and critical dimension (CD) of the PS chemical guides, as well as the annealing temperature, to obtain defect-free sub-10 nm half-pitch line patterns across 1000 μm^2 after 5 min of industrially acceptable thermal annealing without top-coat. A roughness analysis of the resulting line patterns revealed a correlation between the primary BCP structure and the uniformity of the patterns.

Table 1. Characterization of PS-*b*-PGM BCPs.

Sample[a]	M_n [kg mol^{-1}][b]	$Đ$[b]	f_{PS}[c]	PGMA in PGM [mol%][c]
PS-*b*-PGM19-10[d]	19.0	1.03	0.499	10
PS-*b*-PGM26-7	25.9	1.03	0.511	7.4
PS-*b*-PGM25-11	24.9	1.03	0.486	11
PS-*b*-PGM23-11	23.0	1.03	0.520	11

[a] PS-*b*-PGM*X*-*Y* denotes a BCP with a M_n of *X* kg mol^{-1} and *Y* mol% PGMA units in its PGM block; [b] Determined using SEC in THF against PS standards; [c] Determined using ^{1}H NMR spectroscopy in $CDCl_3$; [d] Reported in ref. [51].

2. Results and Discussion

2.1. Perpendicular Windows of the Neutral Layer Composition and BCP Film Thickness

Symmetric PS-*b*-PG_FM BCPs with PGMA contents of 7–11 mol% in the PG_FM block were synthesized by living anionic polymerization (**Table 1**), followed by post-functionalization via a thiol–epoxy reaction (**Table 2**). In our previous study, perpendicular lamellar structures were formed in thin films of PS-*b*-PG_FM with less than 23 mol% PGMA; however, it was difficult to obtain perpendicular lamellae in the entire thin film of PS-*b*-PG_FM with 33 mol% PGMA.[51] The results of the surface free energy (SFE) estimation for the PG_FM showed that the PG_FM containing ≈10 mol% PGMA had an SFE similar to that of PS. Therefore, in this study, we decided to use PS-*b*-PG_FM with 7–11 mol% PGMA to obtain perpendicular lamellae with high reliability. The synthesis and characterization of PS-*b*-PG_FM are described in the previous study.[51] The resulting polymers exhibited unimodal size-exclusion chromatography (SEC) curves (Figure S1, Supporting Information), indicating successful synthesis without any side reactions. To form lamellar structures with periodic lengths of <20 nm, the molecular weights of the PS-*b*-PGM precursors were adjusted to 19–26 kg mol^{-1}. The morphologies and domain spacings (*d*-spacings) of the microphase-separated structures in the bulk films were determined using small-angle X-ray scattering (SAXS), as shown in Table 2. The SAXS profiles reveal scattering peaks at integer ratios relative to their first-order peaks (q^*), indicating the presence of lamellar structures (Figure S2, Supporting Information). The *d*-spacings of the lamellar structures were calculated using Equation (1), based on the positions of q^*.

$$d = \frac{2\pi}{q*} \tag{1}$$

The synthesized PS-*b*-PG_FM BCPs formed lamellar structures with *d*-spacings of <20 nm, corresponding to line patterns with a sub-10 nm half pitch.

Table 2. Characterization of PS-*b*-PG$_F$M BCPs.

Sample	Precursor	M_n [kg mol^{-1}][a)]	$Đ$[a)]	f_{PS}[b)]	Morphology[c)]	*d*-Spacing [nm][d)]
PS-*b*-PG$_F$M19-10[e)]	PS-*b*-PGM19-10	21.0	1.03	0.497	Lamellar	18.1
PS-*b*-PG$_F$M26-7	PS-*b*-PGM26-7	26.6	1.03	0.518	Lamellar	18.9
PS-*b*-PG$_F$M25-11	PS-*b*-PGM25-11	27.0	1.03	0.494	Lamellar	19.9
PS-*b*-PG$_F$M23-11	PS-*b*-PGM23-11	24.7	1.03	0.530	Lamellar	18.2

[a)] Determined using SEC in THF against PS standards; [b)] Determined using ^{1}H NMR spectroscopy in $CDCl_3$; [c)] Determined using the SAXS peak ratios; [d)] Determined using Equation (1); [e)] Reported in ref. [51].

The perpendicular windows of the neutral layer composition and BCP film thickness were investigated using PS-*b*-PG$_F$M19-10. PS-*b*-PG$_F$M19-10 films with a thickness of 27 nm were prepared on silicon wafers modified with polystyrene-*random*-poly(methyl methacrylate)-*random*-poly(2-hydroxyethyl methacrylate) (PS-*r*-PMMA-*r*-PHEMA) random copolymers of varying compositions, acting as neutral layers. **Figure 1** shows the atomic force microscopy (AFM) phase images of thin films annealed at 200 °C for 5 min. Fingerprint-like patterns indicative of perpendicular lamellae were observed on the neutral layers with PS molar ratios (F_{PS}) between 0.35 and 0.66. To further investigate the perpendicular window of the film thickness, PS-*b*-PG$_F$M thin films of varying thickness (15–140 nm) were applied to wafers modified with PS-*r*-PMMA-*r*-PHEMA with a F_{PS} of 0.50 (NL-50) (**Figure 2**). Perpendicular lamellae were observed even on the surface of the 140 nm thick film after thermal annealing. Cross-sectional scanning electron microscopy (SEM) images of the 94- and 131-nm-thick films revealed that the lamellar structures were perpendicularly oriented in the films (**Figure 3**). Perpendicular lamellae formed with high reproducibility, which was attributed to the compositional gradient in the PG$_F$M block. Jung et al. reported that a decrease in the concentration of components with low surface free energy introduced in PS-*b*-PMMA derivatives from the junction point to the end promoted a perpendicular orientation.[52,53] The concentration of PGMA$_F$ units in PS-*b*-PG$_F$M has been suggested to decrease from the junction point to the end of the polymer chain.

2.2. Temperature Dependence of the Domain Size and Correlation Length

To optimize the annealing conditions for the DSA, the periodic length of the perpendicular lamellae (L_0) and the correlation length (CL) were determined. For the DSA, line patterns with the desired pitches were obtained when L_0 was slightly longer than the target pitch. The CL is a quantitative measure of the degree of order in the direction of microphase-separated

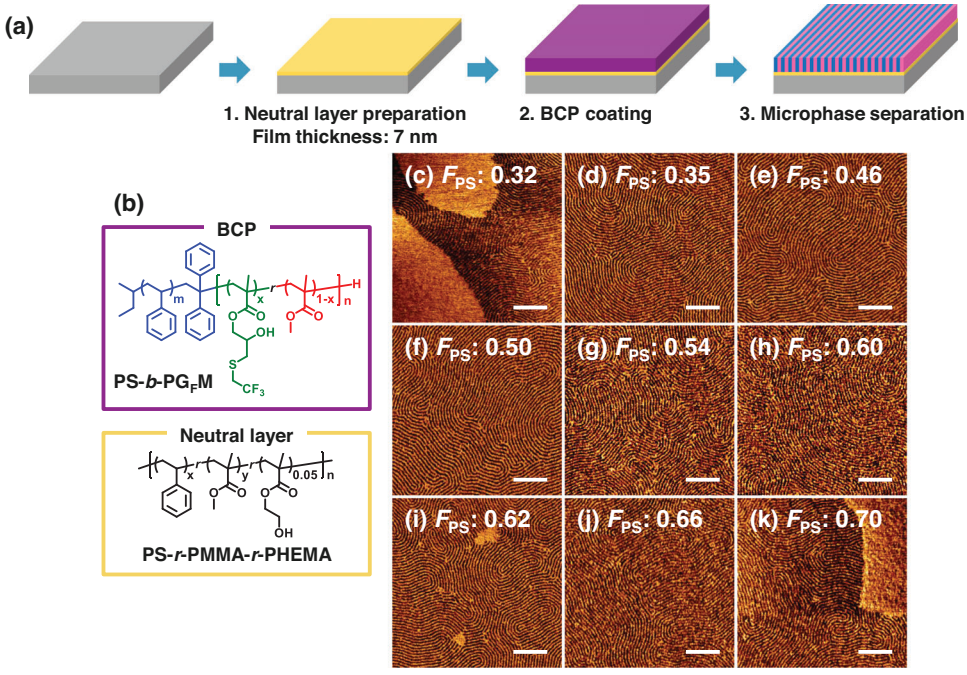

Figure 1. a) Schematic of the general procedure for thin-film studies shown in Figure 1–4. b) Molecular structures of the BCP and random copolymer used for the neutral layers. AFM phase images of PS-*b*-PG$_F$M19-10 thin films with a thickness of 27 nm on silicon wafers modified with random copolymers with F_{PS} of c) 0.32 (NL-32), d) 0.35 (NL-35-1), e) 0.46 (NL-46), f) 0.50 (NL-50), g) 0.54 (NL-54), h) 0.60 (NL-60), i) 0.62 (NL-62), j) 0.66 (NL-66), and k) 0.70 (NL-70). The thin films were annealed at 200 °C for 5 min. The white scale bars represent 200 nm.

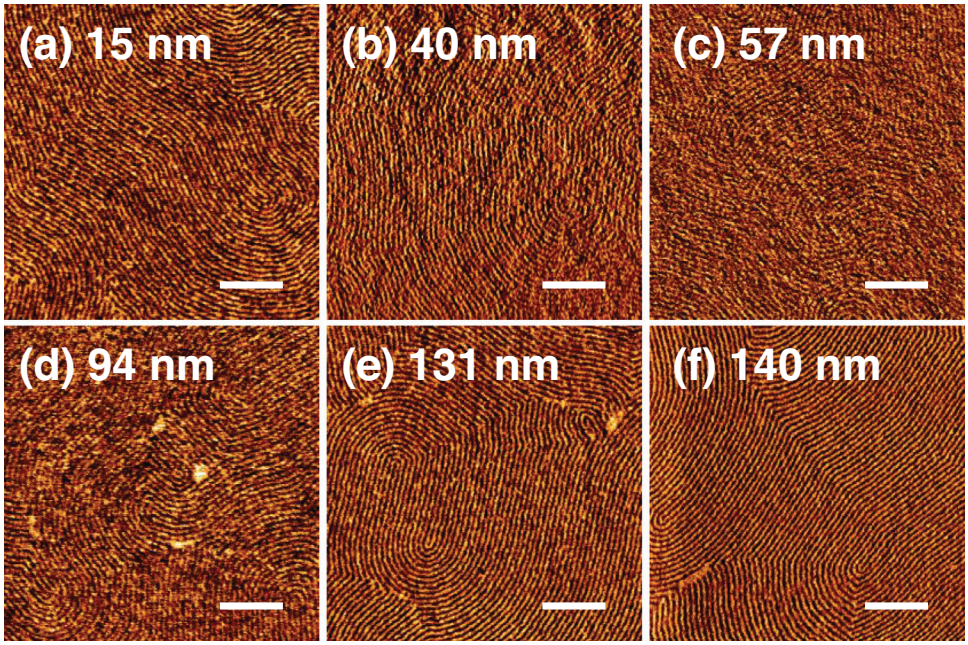

Figure 2. AFM phase images of PS-*b*-PG_FM19-10 thin films with thicknesses of a) 15 nm, b) 40 nm, c) 57 nm, d) 94 nm, e) 131 nm, and f) 140 nm on silicon wafers modified with NL-50 and annealed at 200 °C for 30 min. The white scale bars represent 200 nm.

structures,[54] where high CL values indicate more linear lamellar structures. PS-*b*-PG_FM thin films with a thickness of 36 nm ($2L_0$) to obtain high-aspect-ratio patterns by the pattern-transfer process were prepared on 300 mm silicon wafers modified with NL-44 and annealed at different temperatures for 5 min. In the lithographic process, DSA should be completed in the shortest possible annealing time; in this study, the annealing time was 5 min, as in previous DSA studies using PS-*b*-PMMA.[45,46] L_0 and CL were determined from the critical dimension scanning electron microscopy (CD-SEM) images (Tables S2–S4, Supporting Information). Thin films of PS-*b*-PG_FM26-7, PS-*b*-PG_FM25-11, and PS-*b*-PG_FM23-11 were annealed at varying temperatures in the ranges of 200–250 °C, 200–280 °C, and 200–260 °C, with 10 °C intervals, respectively. As the annealing temperature

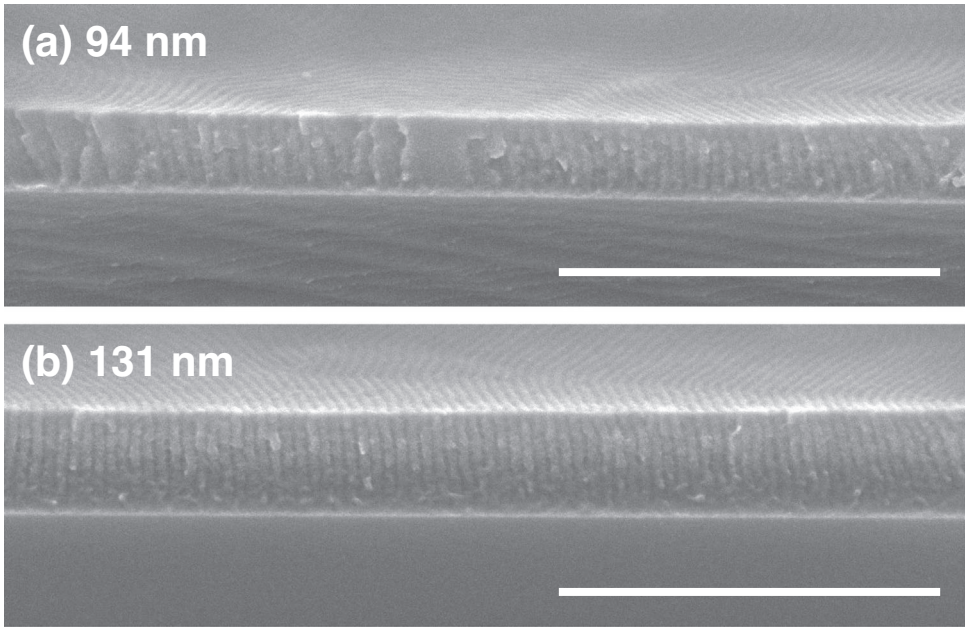

Figure 3. Cross-sectional SEM images of PS-*b*-PG_FM19-10 thin films with thicknesses of a) 94 nm and b) 131 nm on silicon wafers modified with NL-50 and annealed at 200 °C for 30 min. The thin films were stained with RuO_4 and sectioned at room temperature. The white scale bars represent 500 nm.

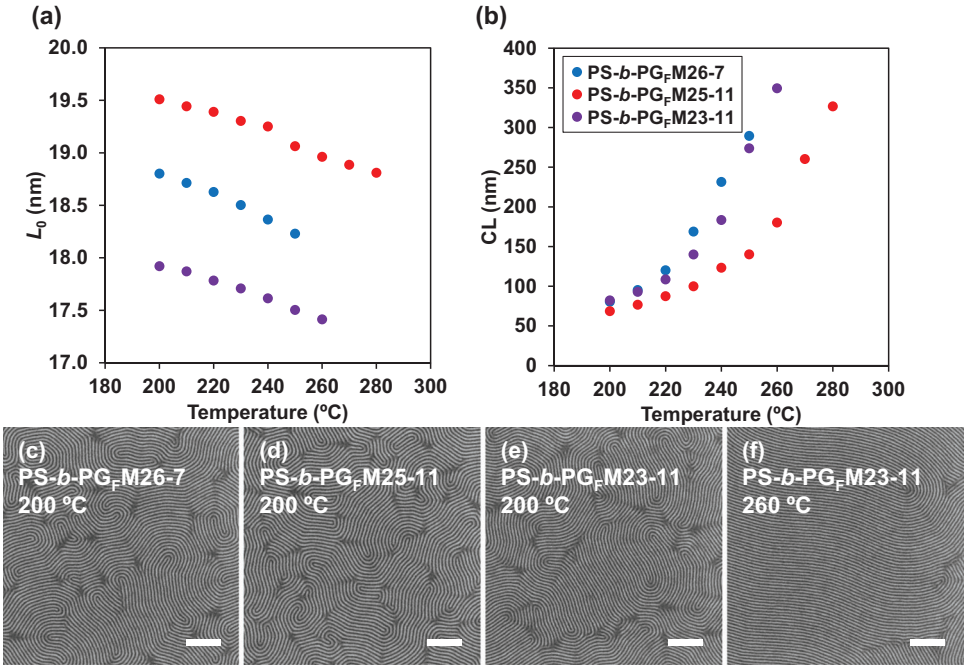

Figure 4. Temperature dependence of a) L_0 and b) CL of PS-*b*-PG$_F$Ms. c–e) Top-down CD-SEM images of c) PS-*b*-PG$_F$M26-7, d) PS-*b*-PG$_F$M25-11, and e) PS-*b*-PG$_F$M23-11 thin films with a thickness of 36 nm on silicon wafers modified with NL-44 and annealed at 200 °C for 5 min. f) Top-down CD-SEM image of PS-*b*-PG$_F$M23-11 thin films with a thickness of 36 nm on silicon wafers modified with NL-44 and annealed at 260 °C for 5 min. The white scale bars represent 200 nm.

increased, the L_0 values of PS-*b*-PG$_F$M26-7, PS-*b*-PG$_F$M25-11, and PS-*b*-PG$_F$M23-11 decreased from 18.8 to 18.2, 19.5 to 18.8, and 17.9 to 17.4 nm, respectively (**Figure 4a**). At higher annealing temperatures, L_0 decreased owing to the thickening of the microdomain interface as the χ values of PS and PG$_F$M decreased[51] and the repulsion between the blocks weakened. On the other hand, PS-*b*-PG$_F$M25-11, and PS-*b*-PG$_F$M23-11 showed dewetting behavior as a result of thermal annealing at 290 and 270 °C for 5 min, respectively (Figure S4, Supporting Information), so DSA was performed at the temperature range in which the perpendicular lamellae formed, as shown in Figure 4.

The CL values of PS-*b*-PG$_F$M26-7, PS-*b*-PG$_F$M25-11, and PS-*b*-PG$_F$M23-11 increased from 80.5 to 289.5, 68.7 to 326.7, and 82.2 to 349.4 nm, respectively, with increasing annealing temperature (Figure 4b–f). Low CL values indicate slow kinetics for the ordering of microphase-separated structures. At higher annealing temperatures, the polymer chains tended to move more freely, forming microphase-separated structures with higher uniformity that resulted in lamellae with less curvature. Higher CL values were advantageous for DSA.

2.3. DSA for Five-Fold Density Multiplication (5× DSA) of PS-*b*-PG$_F$M

2.3.1. Process Windows of the Pitch and Critical Dimension of the PS Chemical Guides for 5× DSA in the PS-b-PG$_F$M Thin Films

Figure 5 shows the general procedure for the 5× DSA. PS chemical guides with different L_s and CD were fabricated using ArF immersion lithography followed by trim etching on silicon wafer-deposited 13 nm-thick silicon nitrides (SiN). The PS chemical guides were created such that their L_s values were five times the pitch of the line patterns in the BCP thin films (L_s = 81–94 nm). After stripping the photoresist, the neutral layers were applied to the patterned wafers. PS-*b*-PG$_F$M thin films with thicknesses of 36 nm were spin-coated onto the wafers and annealed (**Table 3**). After removing the PG$_F$M, four CD-SEM images were captured for each PS chemical guide. **Figure 6** presents the results of the 5× DSA using the PS-*b*-PG$_F$M BCPs. The green circles indicate that line patterns were obtained for all CD-SEM images for the given conditions. The process windows of the 5× DSA expanded and shifted toward lower L_s as the annealing temperature increased, which was attributed to the increase in CL and decrease in L_0 with increasing temperature.

2.3.2. Investigation of Line Pattern Defects

To obtain line patterns with an 18 nm pitch, the current target for high-χ DSA, the higher-order structures on the chemical guides with L_s of 90 nm (18 nm × 5 times) were analyzed in detail. These investigations focused on identifying parallel areas and dislocations (**Figure 7a,b**). The practical implementation of DSA requires that the number of structural defects is less than 1 per 100 cm^2,[55] although defect reduction remains a challenging issue. In this study, the number of parallel areas and dislocations per 1000 μm^2 was evaluated by analyzing 250 SEM images (2 μm × 2 μm) to assess the potential of PS-*b*-PG$_F$M as a DSA material prior to defect inspection on a practical scale. The thin films of PS-*b*-PG$_F$M26-7 annealed at 240 °C and PS-*b*-PG$_F$M25-11 annealed at 270 °C were studied owing to their relatively wider

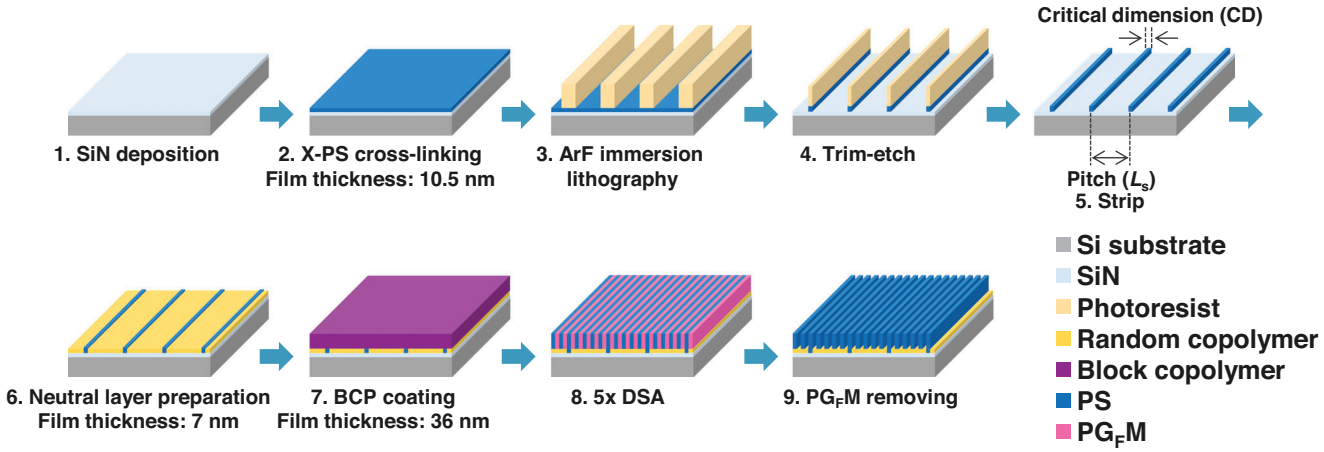

Figure 5. Schematic of the general procedure for the fabrication of chemically patterned silicon wafers and 5× DSA using PS-*b*-PG_FMs.

process windows than those annealed at other temperatures, with L_s values between 89 and 91 nm. Figure 7a,b show the process windows of DSA on PS chemical guides with an L_s of 90 nm to achieve 18 nm line patterns free of parallel areas and dislocations. PS-*b*-PG_FM26-7 and PS-*b*-PG_FM25-11 formed defect-free line patterns over the measured area (1000 μm^2) when the CDs of the PS chemical guides were 15.0–18.7 nm ($0.82L_0$–$1.0L_0$) and 10.7–16.4 nm ($0.57L_0$–$0.87L_0$), respectively. The trends observed in these process windows align with previous findings on 3× DSA using PS-*b*-PMMA with L_0 = 28 nm on PS guides with L_s = 84 nm[56] and 4× DSA using a mixture of ionic liquids and PS-*b*-PMMA with L_0 = 19.3 nm on PS guides with L_s = 78 nm.[57]

2.3.3. Miniaturization of Line Patterns Using Low-Molecular-Weight PS-b-PG_FM

To achieve line patterns with pitches of <18 nm, thin films of PS-*b*-PG_FM23-11 with L_0 below 18 nm were applied to silicon wafers grafted with PS chemical guides (Figure 6g–i). The lowest L_s for successful 5× DSA was 83 nm, indicating that the pitch of the line patterns on the chemical guides was 16.6 nm, corresponding to a half pitch of 8.3 nm. Line patterns annealed at 230 °C on PS chemical guides (L_s = 87 nm) were further investigated

Table 3. Wafer information for 5× DSA.

Sample[a)]	BCP	Annealing temperature [°C]
Wafer-1	PS-*b*-PG_FM26-7	220
Wafer-2	PS-*b*-PG_FM26-7	230
Wafer-3	PS-*b*-PG_FM26-7	240
Wafer-4	PS-*b*-PG_FM25-11	250
Wafer-5	PS-*b*-PG_FM25-11	260
Wafer-6	PS-*b*-PG_FM25-11	270
Wafer-7	PS-*b*-PG_FM23-11	230
Wafer-8	PS-*b*-PG_FM23-11	240
Wafer-9	PS-*b*-PG_FM23-11	250

[a)] Thin films were prepared on patterned silicon wafers grafted with NL-40 and annealed for 5 min.

owing to the relatively wider 5× DSA window with fewer parallel areas than those annealed at other temperatures and other L_s values (Figure 7c). A pitch of 17.4 nm was achieved on PS chemical guides with a CD of 14.0–15.4 nm ($0.79L_0$–$0.87L_0$) without parallel areas or dislocations over the measured area (1000 μm^2). Figure 7a–c shows that as the CD of the PS chemical guide increased or decreased from the optimum value of DSA, parallel lamellae were observed. This is because the interactions of PS and PG_FM with the wafer surface changed as the area of the PS chemical guide changed, and a parallel orientation was induced as a block that selectively acclimated the wafer. As shown in Figure 7a,b, no increase or decrease in dislocation was observed with the change in CD, whereas Figure 7c shows a significant increase in dislocation owing to the change in CD. These results indicate that the first sign of a CD mismatch with DSA is the formation of parallel lamellae, followed by the formation of dislocations. As the molecular weight of the BCPs decreased, the orientation of the microphase-separated structure became increasingly sensitive to variations in the properties of the substrate surface. This implies that more stringent experimental conditions are required to achieve perpendicular orientation. Doise et al. reported that higher CL values help to reduce dislocations[50]; for instance, PS-*b*-PG_FM23-11 annealed at 230 °C exhibited a CL of 140 nm, whereas PS-*b*-PG_FM25-11 annealed at 270 °C displayed a CL of 260 nm. Owing to the relatively low CL value at lower annealing temperatures, PS-*b*-PG_FM23-11 exhibited a significant number of dislocations. By decreasing the thickness of the BCP thin film[50,55] or sufficiently increasing the annealing time,[58] the density of structural defects, particularly dislocations, is expected to decrease.

2.3.4. Roughness Study

Figure 8a–c shows the mean line CD, unbiased line width roughness (uLWR), and unbiased line edge roughness (uLER) of PS-*b*-PG_FM BCPs as a function of the ratio of L_s to L_0. The mean line CDs of PS-*b*-PG_FMs increased with increasing L_s, while uLWR and uLER decreased. The evolution of roughness with L_s, as observed here, differs qualitatively from previous studies on

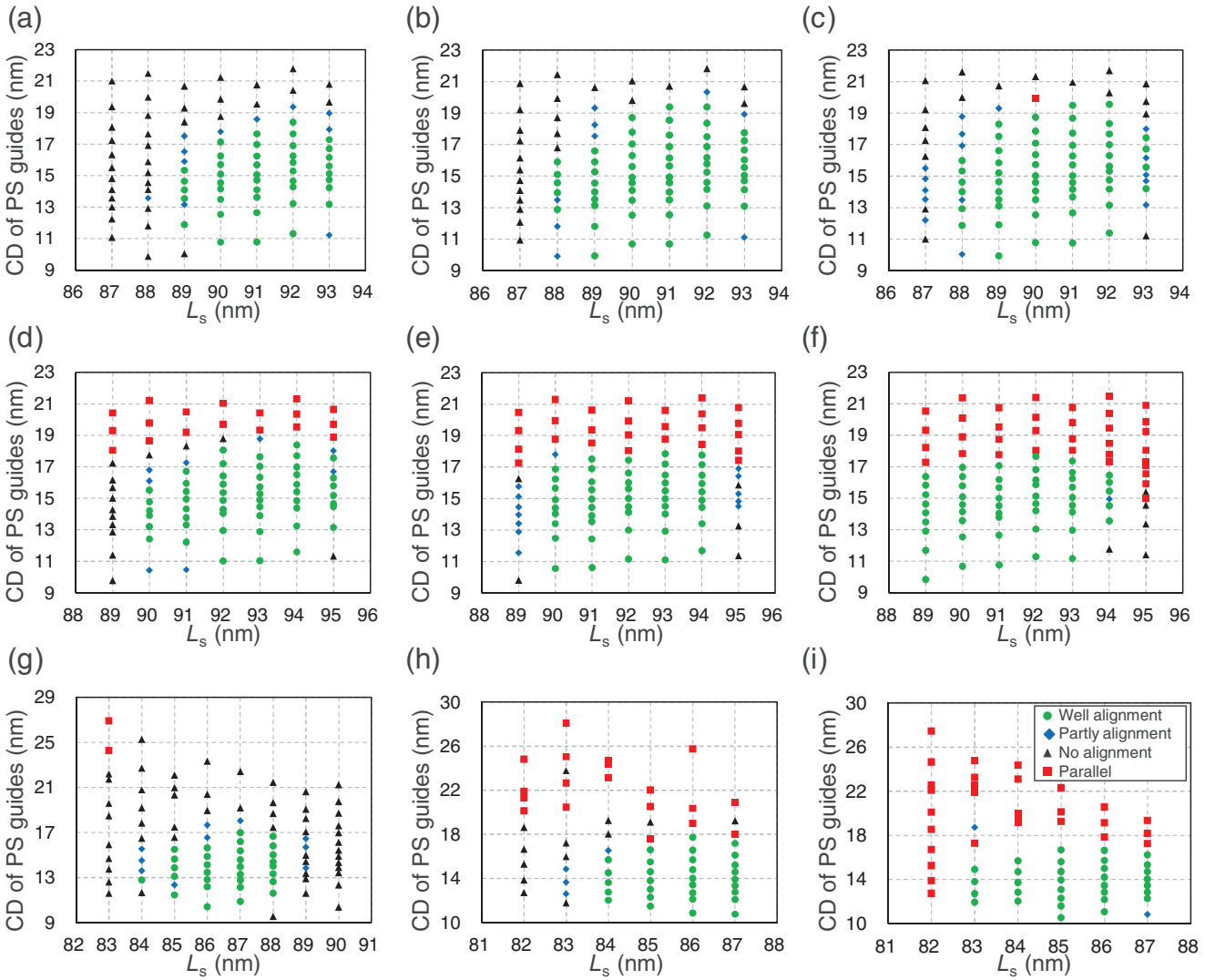

Figure 6. Results of 5× DSA for a) Wafer-1, b) Wafer-2, c) Wafer-3, d) Wafer-4, e) Wafer-5, f) Wafer-6, g) Wafer-7, h) Wafer-8, and i) Wafer-9. Four CD-SEM images were obtained for each condition of the PS chemical guides. The green and blue shapes indicate well-aligned lamellae in all or at least one image, respectively. Black means no alignment, and red indicates parallel orientation in at least one image.

PS-*b*-PMMA.[59] These results are attributed to the repulsion between the blocks. In DSA on the PS chemical guides with lower L_s, both blocks overlap and the interface of the lamellar domain thickens to reduce the periodic length of the lamellar structure to achieve line patterns. The domain interface in the PS-*b*-PG_FM is clearer than that in PS-*b*-PMMA but is expected to be tortuous. The undefined domain interface in PS-*b*-PMMA is etched and shows better roughness, while the curved domain interface in PS-*b*-PG_FM is rougher owing to the selective etching of the PG_FM. On the other hand, as L_s/L_0 increased, the roughness improved because the PS and PG_FM interfaces aligned straightly. This result is also reflected in the slopes of the lines in Figure 8b,c. The absolute values of the slopes are greater for the polymer with 11 mol% $PGMA_F$ than for the polymer with 7 mol% $PGMA_F$, indicating that the curved interfaces straighten as L_s increases. PS-*b*-PG_FM25-11 exhibited better uLWR and uLER values than PS-*b*-PG_FM26-7, as the χ value of PS-*b*-PG_FM increases with the number of $PGMA_F$ units in the PG_FM block.[51] PS-*b*-PG_FM25-11 formed finer domain interfaces than PS-*b*-PG_FM26-7 owing to the higher repulsion between blocks. However, PS-*b*-PG_FM23-11 exhibited the highest uLWR and uLER because it had the thickest lamellar domain interface, which was associated with the smallest χN resulting from the lowest molecular weight. Roughness has been reported to worsen with low L_0 or N in PS-*b*-PMMA,[59] and the results of this study are consistent with the roughness trend of PS-*b*-PMMA.

This study demonstrates that the roughness of high-χ BCPs for L_s/L_0 follows a different trend than that of PS-*b*-PMMA. We propose that controlling higher-order structures based on the primary polymer architecture is crucial for improving roughness. Specifically, the roughness of line patterns in high-χ BCPs should be discussed in terms of χN values. However, this study does not estimate the effective χ value for PS-*b*-PG_FM with 7 mol% $PGMA_F$ and is thus limited to a qualitative discussion

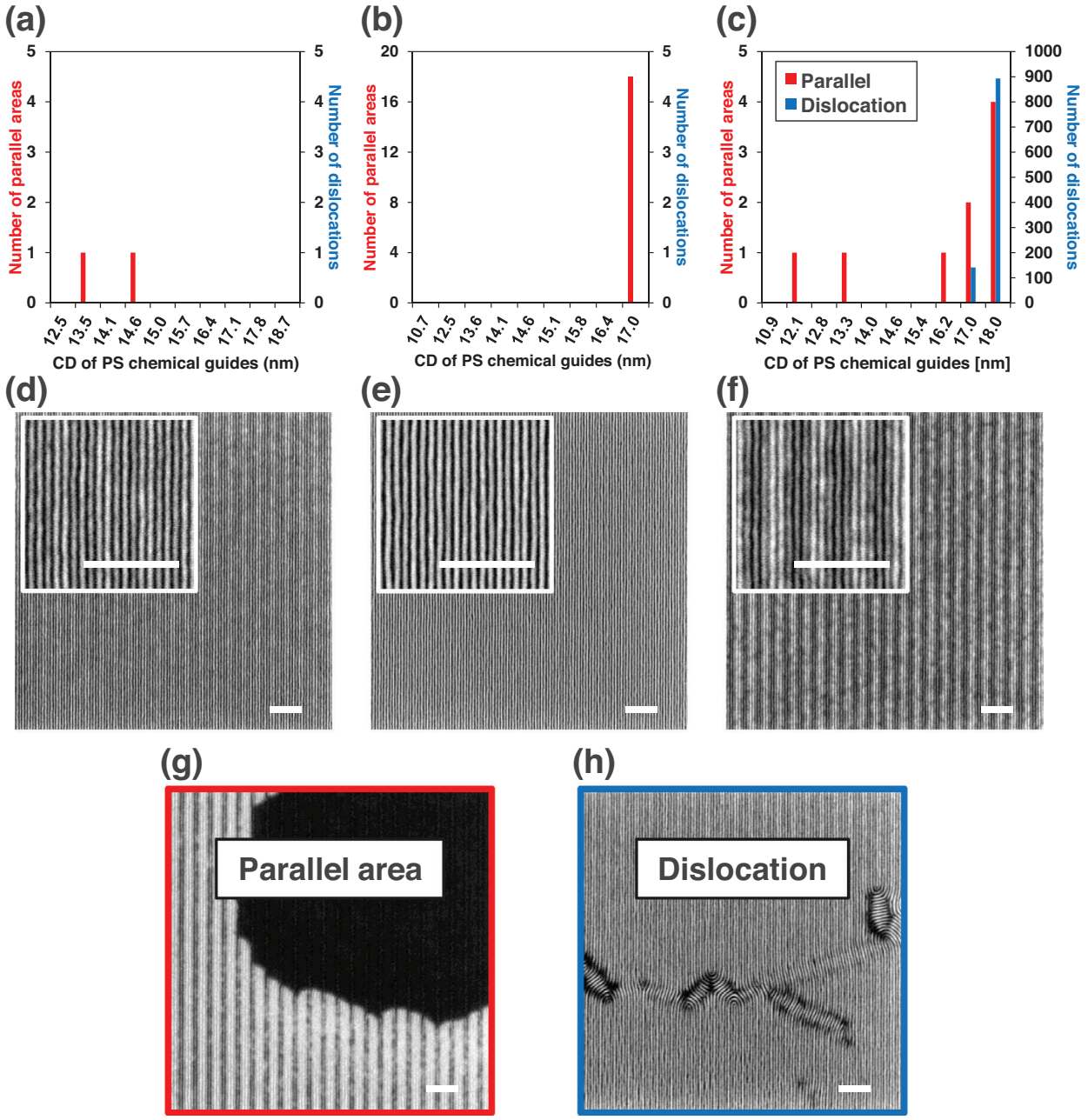

Figure 7. Number of parallel areas and dislocations in a) Wafer-3 at PS chemical guides with L_s = 90 nm, b) Wafer-6 at PS chemical guides with L_s = 90 nm, and c) Wafer-7 at PS chemical guides with L_s = 87 nm. d–f) Top-down SEM images of d) Wafer-3 at PS chemical guides with L_s = 90 nm and 14.1 nm CD, e) Wafer-6 at PS chemical guides with L_s = 90 nm and 14.1 nm CD, and f) Wafer-7 at PS chemical guides with L_s = 87 nm and 14.6 nm CD. g,h) SEM images illustrating g) parallel area and h) dislocation. The white scale bars represent 200 nm.

of the amount of $PGMA_F$ introduced to infer the strength of the repulsive interactions.

3. Conclusion

In conclusion, we demonstrated the DSA of high-χ PS-*b*-PMMA derivatives functionalized with 2,2,2-trifluoroethyl and hydroxy groups to fabricate sub-10 nm half-pitch line patterns free of dislocation defects on 300 mm silicon wafers, using the established DSA process for PS-*b*-PMMA. PS-*b*-PG_FM successfully formed perpendicular lamellae in thin films on PS-*r*-PMMA-*r*-PHEMA random copolymers with PS compositions ranging from 35 to 66 mol%. Perpendicular lamellae were also formed in the BCP films with thicknesses ranging from 15 to 140 nm. These results indicate that PS-*b*-PG_FM reliably forms perpendicularly oriented lamellar structures. During DSA for density multiplication, line patterns with 18 nm pitches— the current target for high-χ DSA—were obtained without parallel areas and disloca-

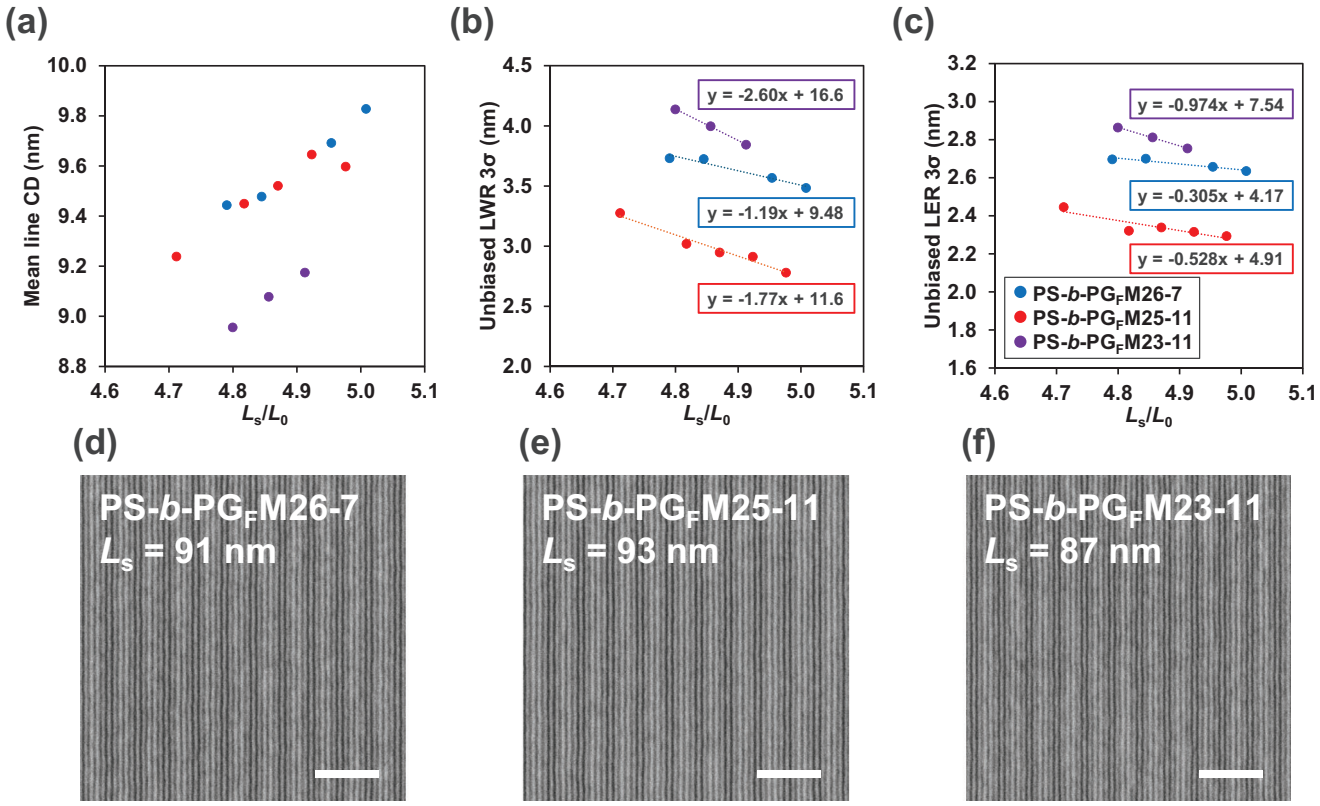

Figure 8. Comparison of a) mean line CD, b) uLWR, and c) uLER of PS-*b*-PG$_F$M BCPs. d–f) Top-down CD-SEM images of d) Wafer-3 at PS chemical guides with L_s = 91 nm and 15.7 nm CD, e) Wafer-6 at PS chemical guides with L_s = 93 nm and 14.5 nm CD, and f) Wafer-7 at PS chemical guides with L_s of 87 nm and 14.0 nm CD. The white scale bars represent 200 nm.

tions. In this study, we achieved line patterns with a half pitch of 8.3 nm. The uLWR and uLER improved with increasing L_s/L_0 and χN. While several high-χ BCPs have been reported to produce line patterns with a sub-10 nm half pitch, reducing the number of dislocation defects is still one of the most important challenges. Thus, we believe that the PS-*b*-PG$_F$M is a promising material for the fabrication of sub-10 nm half-pitch line-and-space patterns via DSA on an industrial scale.

4. Experimental Section

Preparation of Thin Films for Investigation of Perpendicular Window: Thin films for investigating the perpendicular window were prepared following a method similar to that described in a previous study.[51] Silicon wafers, either cut to dimensions of 1.5 × 1.5 cm or a diameter of 1.5 cm, were wiped with toluene-soaked Kimwipes. The wafers were then sequentially sonicated in acetone, ethanol, and toluene (1 min each), dried under a nitrogen stream, and further dried by heating to 100 °C. Random copolymer layers were prepared on the cleaned wafers by spin coating 1 wt.% PS-*r*-PMMA-*r*-PHEMA solution in propylene glycol 1-monomethyl ether 2-acetate (PGMEA) at 3000 rpm for 60 s, followed by crosslinking at 250 °C for 5 min under a nitrogen atmosphere. Subsequent rinsing with PGMEA removed the uncrosslinked random copolymers to yield PS-*r*-PMMA-*r*-PHEMA layers ≈ 5–7 nm thick, which neutralized the surfaces of the silicon wafers. The modified wafers were sufficiently dried by heating at 100 °C for 1 min. Thin films were fabricated by spin coating BCP solutions at the given concentrations in PGMEA at varying spin rates for 60 s to obtain thin films of varying thickness. The BCP thin films were first heated to 90 °C for 1 min to remove residual PGMEA, followed by annealing at 200 °C for 5 or 30 min under a nitrogen atmosphere.

Preparation of Thin Films for L_0 and CL Measurements: L_0 and CL measurements were conducted on a 300 mm wafer process line at IMEC, Belgium. Silicon wafers were dried by heating at 100 °C for 1 min. PS-*r*-PMMA-*r*-PHEMA was spin coated onto the wafers from the PGMEA solution and cross-linked at 250 °C for 5 min in a nitrogen atmosphere. The uncrosslinked PS-*r*-PMMA-*r*-PHEMA was rinsed with PGMEA, leaving 7.3 nm thick neutral layers. PS-*b*-PG$_F$M thin films with thicknesses of 36 nm were spin coated onto surface-neutralized wafers. The thin-film samples were heated at 100 °C for 1 min and then annealed at varying temperatures for 5 min. The PG$_F$M domains were removed by dry etching prior to SEM characterization.

5× DSA Using PS-b-PG$_F$M: The thin-film studies were performed on a 300 mm wafer process line at IMEC, Belgium. SiN layers of 13 nm thickness were deposited onto 300 mm silicon wafers. The wafers were heated to 350 °C for 1 min. X-PS was spin coated onto the wafers, forming films with a thickness of 10.5 nm, and cross-linked at 315 °C for 5 min under a nitrogen atmosphere. The wafers were coated with AIM5484 photoresist with a thickness of 95 nm, followed by patterning using ArF immersion lithography. The resist patterns were transferred to the X-PS layer to create line-and-space patterns with varying L_s and CD. After photoresist stripping, the silicon wafers were dried by heating at 100 °C for 1 min. PS-*r*-PMMA-*r*-PHEMA was spin coated onto the wafers from the PGMEA solution and cross-linked at 250 °C for 5 min in a nitrogen atmosphere. The uncrosslinked PS-*r*-PMMA-*r*-PHEMA was rinsed with PGMEA, leaving a 7.3 nm thick neutral layer. Then, 36 nm thick films of PS-*b*-PG$_F$M were spin coated onto the patterned wafers. The thin-film samples were heated at 100 °C for 1 min and annealed at varying temperatures for 5 min in a nitrogen atmosphere. The PG$_F$M domains were removed by dry etching prior to SEM measurements.

Image Analysis: For the determination of L_0 values, the following imaging conditions were used: *magnification*, 100 000; *pixels*, 2048 × 2048; *number of frames*, 16; and *number of images*, 20. The L_0 values were extracted using DSA-APPS (Hitachi High Tech), and the average number from 20 images was reported. The following imaging conditions were used to determine the CL values: *magnification*, 25 000; *pixels*, 2048 × 2048; *number of frames*, 16; *number of images*, 36. The CL was extracted using an in-house-developed image-processing algorithm using the ImageJ open-source software package, and the average number from 36 images was reported. For defect analysis, a total of 250 SEM images (2 µm × 2 µm) were taken for different CD values of the chemical guides with a target L_s of 87 or 90 nm, and the number of parallel areas and dislocations were manually counted. To extract the roughness, the following imaging conditions were chosen: *magnification*, 132 000; *pixels*, 2048 × 2048; *number of frames*, 16; and *number of images*, ≥41. Metrology was performed via offline image analysis using MetroLER$_{TM}$ version 4.1.0.0 (Fractilia, LCC).

Supporting Information

Supporting Information is available from the Wiley Online Library or from the author.

Acknowledgements

The manuscript was written with contributions from all the authors. All the authors approved the final version of the manuscript. The authors thank Dr. Noboru Ohta (JASRI) and Prof. Tomoyasu Hirai (Osaka Institute of Technology) for SAXS measurements at the BL40B2 beamline of SPring-8 (Proposal no. 2024A1166). The authors also thank Ryohei Kikuchi (Core Facility Center, Institute of Science Tokyo) for the TEM and cross-sectional SEM support. This work was supported by JSPS KAKENHI (grant numbers 20H02785 and 24H00052). S. M. was supported by JST SPRING (grant numbers: JPMJSP2106 and JPMJSP2180).

Conflict of Interest

The authors declare no conflict of interest.

Data Availability Statement

The data that support the findings of this study are available on request from the corresponding author. The data are not publicly available due to privacy or ethical restrictions.

Keywords

block copolymers, directed self-assembly, high-chi polymers, lithography, microphase separation, thin films

Received: November 2, 2024
Revised: December 23, 2024
Published online: February 12, 2025

[1] T. Allenet, X. Wang, M. Vockenhuber, C.-K. Yeh, I. Mochi, J. G. Santaclara, L. Van Lent-Protasova, Y. Ekinci, *Proc. SPIE* **2021**, *11609*, 116090J.
[2] IEEE, *International Roadmap for Devices and Systems*^{TM} *2022 Edition Lithography*, https://irds.ieee.org/images/files/pdf/2022/2022IRDS_Litho.pdf, (accessed: October 2024).
[3] Y.-J. Kwark, J. P. Bravo-Vasquez, H. B. Cao, H. Deng, C. K. Ober, *J. Photopolym. Sci. Technol.* **2005**, *18*, 481.
[4] M. Trikeriotis, W. J. Bae, E. Schwartz, M. Krysak, N. Lafferty, P. Xie, B. Smith, P. A. Zimmerman, C. K. Ober, E. P. Giannelis, *Proc. SPIE* **2010**, *7639*, 76390E.
[5] M. Trikeriotis, M. Krysaki, Y. S. Chung, C. Ouyang, B. Cardineau, R. Brainard, C. K. Ober, E. P. Giannelis, K. Cho, *J. Photopolym. Sci. Technol.* **2012**, *25*, 583.
[6] F. Kaefer, Z. Meng, R. Segalman, C. K. Ober, *J. Photopolym. Sci. Technol.* **2022**, *35*, 29.
[7] F. Käfer, C. Wang, Y. Huang, F. Bard, R. Segalman, C. K. Ober, *Adv. Mater. Technol.* **2023**, *8*, 2301104.
[8] C. K. Ober, F. Käfer, C. Yuan, *Polymer* **2023**, *280*, 126020.
[9] J. K. Stowers, A. Telecky, M. Kocsis, B. L. Clark, D. A. Keszler, A. Grenville, C. N. Anderson, P. P. Naulleau, *Proc. SPIE* **2011**, *7969*, 796915.
[10] Y. Ekinci, M. Vockenhuber, M. Hojeij, L. Wang, N. M. Mojarad, *Proc. SPIE* **2013**, *8679*, 867910.
[11] Line Edge Roughness, part, 1, https://www.lithoguru.com/scientist/litho_tutor/Tutor56%20(Feb%2007).pdf, (accessed: October 2024).
[12] P. De Bisschop, J. Van de Kerkhove, J. Mailfert, A. Vaglio Pret, J. Biafore, *Proc. SPIE* **2014**, *9048*, 904809.
[13] A. Chunder, A. Latypov, Y. Chen, J. J. Biafore, H. J. Levinson, T. Bailey, *Proc. SPIE* **2017**, *10146*, 101460B.
[14] T. Fujimori, *J. Photopolym. Sci. Technol.* **2022**, *35*, 35.
[15] IEEE, *International Roadmap for Devices and Systems*^{TM} *2023 Update Lithography & Patterning*, https://irds.ieee.org/images/files/pdf/2023/2023IRDS_Litho.pdf, (accessed: October 2024).
[16] R. Ruiz, H. Kang, F. A. Detcheverry, E. Dobisz, D. S. Kercher, T. R. Albrecht, J. J. de Pablo, P. F. Nealey, *Science* **2008**, *321*, 936.
[17] M. P. Stoykovich, K. C. Daoulas, M. Müller, H. Kang, J. J. de Pablo, P. F. Nealey, *Macromolecules* **2010**, *43*, 2334.
[18] C. Oh, J. Kim, J. Heo, H. Seo, K. An, C. Bok, M. Kim, S. Park, *J. Photopolym. Sci. Technol.* **2013**, *26*, 595.
[19] R. Gronheid, A. Singh, T. R. Younkin, P. R. Delgadillo, P. Nealey, B. T. Chan, K. Nafus, A. R. Negreira, M. Somervell, *Proc. SPIE* **2013**, *8682*, 86820A.
[20] L. Verstraete, H. S. Suh, J. Van Bel, P. H. Timi, R. Vallat, P. Bezard, J. Vandereyken, M. Beggiato, A.-H. Tamaddon, C. Beral, W. Li, M. Gupta, R. Fallica, *Proc. SPIE* **2023**, *12497*, 124970I.
[21] J. Van Bel, L. Verstraete, H. S. Suh, S. De Gendt, P. Bezard, J. Vandereyken, W. Li, M. Beggiato, A.-H. Tamaddon, C. Beral, A. Santos, B. Alperson, Y. Her, *Proc. SPIE* **2023**, *12497*, 124970K.
[22] L. Verstraete, H. S. Suh, J. Van Bel, B.-U. Bak, S. E. Kim, R. Vallat, P. Bezard, M. Beggiato, C. Beral, *Proc. SPIE* **2024**, *12956*, 129560G.
[23] C.-C. Liu, C. J. Thode, P. A. R. Delgadillo, G. S. W. Craig, P. F. Nealey, R. Gronheid, *J. Vac. Sci. Technol. B* **2011**, *29*, 06F203.
[24] G.-W. Yang, G.-P. Wu, X. Chen, S. Xiong, C. G. Arges, S. Ji, P. F. Nealey, X.-B. Lu, D. J. Darensbourg, Z.-K. Xu, *Nano Lett.* **2017**, *17*, 1233.
[25] X. Zhang, Q. He, Q. Chen, P. F. Nealey, S. Ji, *ACS Macro Lett.* **2018**, *7*, 751.
[26] F. S. Bates, G. H. Fredrickson, *Annu. Rev. Phys. Chem.* **1990**, *41*, 525.
[27] M. W. Matsen, F. S. Bates, *Macromolecules* **1996**, *29*, 1091.
[28] C. Sinturel, F. S. Bates, M. A. Hillmyer, *ACS Macro Lett.* **2015**, *4*, 1044.
[29] P. Mansky, P. Chaikin, E. L. Thomas, *J. Mater. Sci.* **1995**, *30*, 1987.
[30] P. Mansky, C. K. Harrison, P. M. Chaikin, R. A. Register, N. Yao, *Appl. Phys. Lett.* **1996**, *68*, 2586.
[31] M. Park, C. Harrison, P. M. Chaikin, R. A. Register, D. H. Adamson, *Science* **1997**, *276*, 1401.
[32] C.-C. Liu, P. F. Nealey, Y.-H. Ting, A. E. Wendt, *J. Vac. Sci. Technol. B* **2007**, *25*, 1963.
[33] R. A. Segalman, H. Yokoyama, E. J. Kramer, *Adv. Mater.* **2001**, *13*, 1152.

[34] S.-M. Park, M. P. Stoykovich, R. Ruiz, Y. Zhang, C. T. Black, P. F. Nealey, *Adv. Mater.* **2007**, *19*, 607.
[35] E. Han, H. Kang, C.-C. Liu, P. F. Nealey, P. Gopalan, *Adv. Mater.* **2010**, *22*, 4325.
[36] T. L. Morkved, M. Lu, A. M. Urbas, E. E. Ehrichs, H. M. Jaeger, P. Mansky, T. P. Russell, *Science* **1996**, *273*, 931.
[37] R. J. Albalak, E. L. Thomas, *J. Polym. Sci., B:Polym. Phys.* **1994**, *32*, 341.
[38] C. Tang, A. Tracz, M. Kruk, R. Zhang, D.-M. Smilgies, K. Matyjaszewski, T. Kowalewski, *J. Am. Chem. Soc.* **2005**, *127*, 6918.
[39] C. Tang, W. Wu, D.-M. Smilgies, K. Matyjaszewski, T. Kowalewski, *J. Am. Chem. Soc.* **2011**, *133*, 11802.
[40] L. Rockford, Y. Liu, P. Mansky, T. P. Russell, M. Yoon, S. G. J. Mochrie, *Phys. Rev. Lett.* **1999**, *82*, 2602.
[41] S. O. Kim, H. H. Solak, M. P. Stoykovich, N. J. Ferrier, J. J. de Pablo, P. F. Nealey, *Nature* **2003**, *424*, 411.
[42] M. P. Stoykovich, M. Müller, S. O. Kim, H. H. Solak, E. W. Edwards, J. J. de Pablo, P. F. Nealey, *Science* **2005**, *308*, 1442.
[43] C.-C. Liu, E. Han, M. S. Onses, C. J. Thode, S. Ji, P. Gopalan, P. F. Nealey, *Macromolecules* **2011**, *44*, 1876.
[44] P. Mansky, T. P. Russell, C. J. Hawker, J. Mays, D. C. Cook, S. K. Satija, *Phys. Rev. Lett.* **1997**, *79*, 237.
[45] P. A. R. Delgadillo, R. Cronheid, C. J. Thode, H. Wu, Y. Cao, M. Neisser, M. Somervell, K. Nafus, P. F. Nealey, *J. Micro/Nanolith. MEMS MOEMS* **2012**, *11*, 031302.
[46] L. Wan, R. Ruiz, H. Gao, K. C. Patel, T. R. Albrecht, J. Yin, J. Kim, Y. Cao, G. Lin, *ACS Nano* **2015**, *9*, 7506.
[47] S. Kim, P. F. Nealey, F. S. Bates, *Nano Lett.* **2014**, *14*, 148.
[48] A. P. Lane, X. Yang, M. J. Maher, G. Blachut, Y. Asano, Y. Someya, A. Mallavarapu, S. M. Sirard, C. J. Ellison, C. G. Willson, *ACS Nano* **2017**, *11*, 7656.
[49] M. J. Maher, C. T. Rettner, C. M. Bates, G. Blachut, M. C. Carlson, W. J. Durand, C. J. Ellison, D. P. Sanders, J. Y. Cheng, C. G. Willson, *ACS Appl. Mater. Interfaces.* **2015**, *7*, 3323.
[50] J. Doise, J. H. Koh, J. Y. Kim, Q. Zhu, N. Kinoshita, H. S. Suh, P. R. Delgadillo, G. Vandenberghe, C. G. Willson, C. J. Ellison, *ACS Appl. Mater. Interfaces.* **2019**, *11*, 48419.
[51] S. Maekawa, T. Seshimo, T. Dazai, K. Sato, K. Hatakeyama-Sato, Y. Nabae, T. Hayakawa, *Nat. Commun.* **2024**, *15*, 5671.
[52] S. W. Song, Y. H. Hur, Y. Park, E. N. Cho, H. J. Han, H. Jang, J. Oh, G. Yeom, J. Lee, K.-S. Yoon, C.-M. Park, I. Kim, Y. Kim, Y. S. Jung, *J. Mater. Chem. C* **2021**, *9*, 14021.
[53] Y. Park, S. W. Song, J. Hong, H. Jang, G. R. Lee, G. Y. Kim, Y. S. Jung, *ACS Macro Lett.* **2024**, *13*, 943.
[54] C. Harrison, P. M. Chaikin, D. A. Huse, R. A. Register, D. H. Adamson, A. Daniel, E. Huang, P. Mansky, T. P. Russell, C. J. Hawker, D. A. Egolf, I. V. Melnikov, E. Bodenschatz, *Macromolecules* **2000**, *33*, 857.
[55] J. Ren, C. Zhou, X. Chen, M. Dolejsi, G. S. W. Craig, P. A. Rincon Delgadillo, T. Segal-Peretz, P. F. Nealey, *ACS Appl. Mater. Interfaces.* **2018**, *10*, 23414.
[56] P. A. Rincon Delgadillo, *PhD Thesis*, University of Chicago, Chicago, IL, USA **2014**.
[57] X. Chen, C. Zhou, S.-J. Chen, G. S. W. Craig, P. Rincon-Delgadillo, T. Dazai, K. Miyagi, T. Maehashi, A. Yamazaki, R. Gronheid, M. P. Stoykovich, P. F. Nealey, *ACS Appl. Mater. Interfaces.* **2018**, *10*, 16747.
[58] J. Li, P. A. Rincon-Delgadillo, H. S. Suh, G. Mannaert, P. F. Nealey, *ACS Appl. Mater. Interfaces.* **2021**, *13*, 25357.
[59] H. S. Suh, V. Dudash, G. Lorusso, C. Mack, *Proc. SPI* **2020**, *11326*, 113260X.